Open Access

Research Article

PRNANO

Precis. Nanomed. 2023, 6(4):1157-1172

ANDOVER HOUSE

A Synergetic Approach Utilizing Nanotechnology, Chemotherapy, and Radiotherapy for Pancreatic Cancer Treatment

Abdulaziz Alhussan[1], Reinali Calisin[1], Nolan Jackson[1], Jessica Morgan[2,3], Sam Chen[4], Yuen Yi C. Tam[4], Wayne Beckham[1,5], Sunil Krishnan[6], Devika B. Chithrani[1,5,7,8, 9*]

[1] *Department of Physics and Astronomy, University of Victoria, Victoria, BC V8P 5C2, Canada;*
[2] *Department of Biochemistry and Microbiology, University of Victoria, Victoria, BC V8P 5C2, Canada;*
[3] *Trev and Joyce Deeley Research Centre, British Columbia Cancer -Victoria, Victoria, BC V8R 6V5, Canada*
[4] *Integrated Nanotherapeutics Inc., Burnaby, BC V5G 4X4, Canada*
[5] *Radiation Oncology, British Columbia Cancer-Victoria, Victoria, BC V8R 6V5, Canada*
[6] *University of Texas Health Science Center at Houston, Vivian L. Smith Department of Neurosurgery, Houston, Texas 77030, United States*
[7] *Centre for Advanced Materials and Related Technologies, Department of Chemistry, University of Victoria, Victoria, BC V8P 5C2, Canada*
[8] *Department of Medical Sciences, University of Victoria, Victoria, BC V8P 5C2, Canada*
[9] *Department of Computer Science, Mathematics, Physics and Statistics, Okanagan Campus, University of British Columbia, Kelowna, BC V1V 1V7, Canada*

Submitted: October 6, 2023 Accepted: November 19, 2023 Published: November 22, 2023

Graphical Abstract

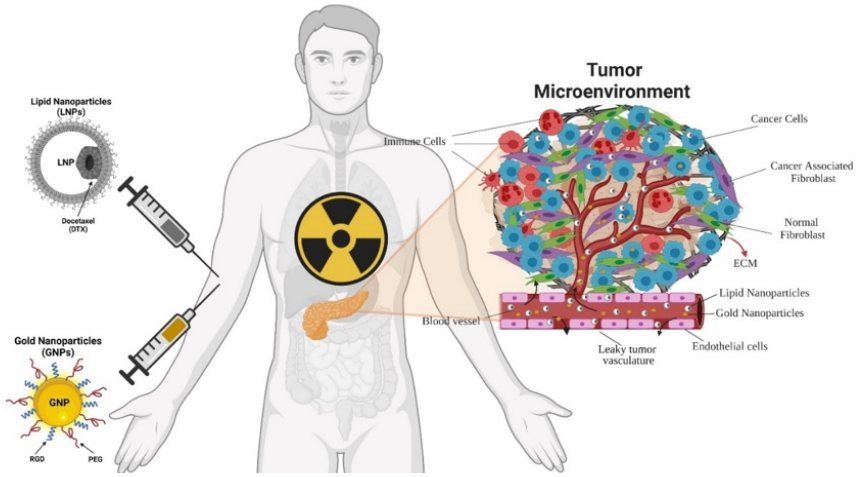

Abstract

The objective of this study was to assess the anticancer effectiveness of gold nanoparticles (GNPs) and lipid-encapsulated docetaxel prodrug ($LNP_{DTX\text{-}P}$) with radiotherapy (RT). The study utilized a co-culture spheroid model comprising MIA PaCa-2 cancer cells and patient-derived cancer-associated fibroblasts (CAF-98) to mimic pancreatic cancer conditions. The spheroids underwent treatment with GNPs (7.5 µg/mL), $LNP_{DTX\text{-}P}$ (99 nM of DTX prodrug), and 2 Gy of RT. Cell viability of the spheroids was evaluated using the CellTiter-Glo 3D assay At the same time, DNA double-strand breaks. (DSBs) were assessed by examining the expression of the DNA damage marker 53BP1 through an immunofluorescence assay. Although GNPs/RT and RT/$LNP_{DTX\text{-}P}$ showed a reduction in spheroid size and an apparent increase in DNA DSB damage, the combination of the two nanoparticles, GNPs, and $LNP_{DTX\text{-}P}$, with RT, significantly enhanced the anticancer efficacy, resulting in a 28% decrease in spheroid size and an estimated 39% increase in DNA DSB. The combination of GNPs and $LNP_{DTX\text{-}P}$ with RT showed a synergetic effect due to their radiosensitizing properties, improving the therapeutic efficacy of each

*Corresponding author: devikac@uvic.ca

treatment modality alone. This triple modality offers a hopeful strategy to enhance cancer treatment efficacy while reducing adverse effects.

Keywords:
Gold Nanoparticles, Docetaxel, Lipid Nanoparticles, Radiotherapy, Pancreatic Cancer.

Rationale, Purpose, and Limitations

This study is motivated by the need to improve the efficacy of cancer treatments, particularly in the context of pancreatic cancer. It focuses on assessing the anticancer effectiveness of gold nanoparticles (GNPs), lipid-encapsulated docetaxel prodrug ($LNP_{DTX\text{-}P}$), and radiotherapy (RT), which could potentially offer better treatment outcomes with reduced side effects. The goal is to establish whether the synergistic combination of these treatments can significantly enhance anticancer efficacy using a co-culture spheroid model. The study is limited by its *in vitro* nature. Further, *in vivo* testing would be necessary to validate these findings before moving to clinical trials.

Introduction

Pancreatic cancer is associated with one of the lowest survival rates among all types of cancer. The five-year survival rate for pancreatic cancer is less than 10% [1]. This form of cancer is a significant global health concern, with 458,918 new cases and 432,242 deaths reported worldwide in 2018, ranking it as the seventh most common cancer and the fourth deadliest [2]. Current treatment approaches for pancreatic cancer heavily depend on the cancer stage and location, typically involving surgery, chemotherapy, and radiotherapy (RT), each with its limitations [3]. Surgical resection followed by adjuvant chemotherapy using FOLFIRINOX or gemcitabine/nab-paclitaxel is considered the most favorable option for early-stage pancreatic cancer [4]. However, due to its invasive nature and high tendency for metastasis, the majority of patients are deemed unsuitable for surgery [5]. A key challenge in chemotherapy lies in the limited drug delivery to tumor sites when using free drugs, resulting in inadequate drug concentrations at the tumor compared to healthy organs [6]. This is influenced by factors like systemic distribution, drug clearance, and the tumor microenvironment (TME) presence, which hold back effective drug delivery to the tumor site [7].

On the other hand, Radiotherapy (RT) plays a crucial role in the curative treatment of various locally advanced non-metastatic cancers, such as breast, prostate, cervix, head and neck, lung, and brain. Approximately 50% of cancer patients currently receive RT as part of their treatment [8]. However, targeting pancreatic cancer with RT is challenging due to its proximity to multiple organs, which limits the desired radiation dose required for local control and may lead to toxicity in nearby healthy tissues [9]. Urgent action is necessary to address the challenges associated with pancreatic cancer and improve outcomes for affected patients.

The field of nanotechnology has emerged as a promising avenue for tackling the obstacles posed by conventional cancer treatments. Nanoparticles (NPs) can be designed for drug delivery using either passive or active targeting mechanisms. Passive targeting relies on the natural properties of tumors to accumulate NPs, while active targeting involves specific interactions between the NPs and molecular targets on tumor cells. NPs have exhibited considerable potential as radiosensitizers in RT and as carriers for precision drug delivery in chemotherapy [10–12]. Among these NPs, gold nanoparticles (GNPs) have emerged as a particularly effective tool for maximizing radiation doses to targeted tumors while minimizing radiation exposure to surrounding healthy tissues [13–16]. GNPs as radiosensitizers can be improved by modifying the surface of NPs with ligands that can specifically bind to receptors overexpressed on the surface of cells in the TME. This active targeting was achieved by functionalizing GNPs with polyethylene glycol (PEG) to decrease immune system recognition and RGD due to its highly selective targeting of cancer cells [15].

On the other hand, lipid nanoparticles (LNPs) are nanoscale structures made up of lipids such as phospholipids and cholesterol that can effectively encapsulate and deliver various types of drugs [17]. In cancer therapy, LNPs have been combined with the chemotherapy drug docetaxel (DTX) to improve treatment efficacy [18]. DTX is an FDA-approved chemotherapy drug that is used to treat various types of cancers, including breast, lung, and prostate cancer [19].

However, it has poor solubility in water, making its delivery to the tumor site difficult [20]. Passive entrapment of DTX with LNPs results in low entrapment because DTX does not have sufficient hydrophobicity to stay associated with the nanoparticle. This leads to dissociated pharmacokinetics of nanoparticles and drugs [21]. This solubility issue can be resolved by encapsulating DTX prodrugs within LNPs. This can improve its accumulation in the tumor passively via the enhanced retention and permeability effect (EPR), increase its effectiveness, and reduce its side effects [21]. Additional advantages of using LNPs with prodrugs of DTX ($LNP_{DTX\text{-}P}$) in cancer therapy include increased drug stability, which allows for longer circulation periods, thus improving overall tumor efficacy [22].

Furthermore, although not done in this experiment, these LNPs can be engineered to selectively target cancer cells, similar to what was done with GNPs, thus enhancing the delivery of DTX directly into cancer cells [23]. This targeted delivery reduces the risk of toxicity to healthy tissues, reducing side effects. The use of LNPs with DTX prodrugs has been shown to reduce the systemic toxicity associated with DTX [24]. Studies have also shown that using LNPs with DTX prodrugs can increase the drug's effectiveness in killing cancer cells, improving overall treatment outcomes [25]. Although DTX is not currently being used to treat pancreatic cancer, given that the mechanism of action of DTX is like that of nab-paclitaxel, combined with its radiosensitizing effects and its tolerable usage with RT, we believe that DTX is a good candidate for this experiment. To comprehensively investigate the combined effects of GNPs, RT, and $LNP_{DTX\text{-}P}$, we used an *in vitro* 3D spheroid model of MIA PaCa-2 cells and pancreatic patient-derived CAFs.

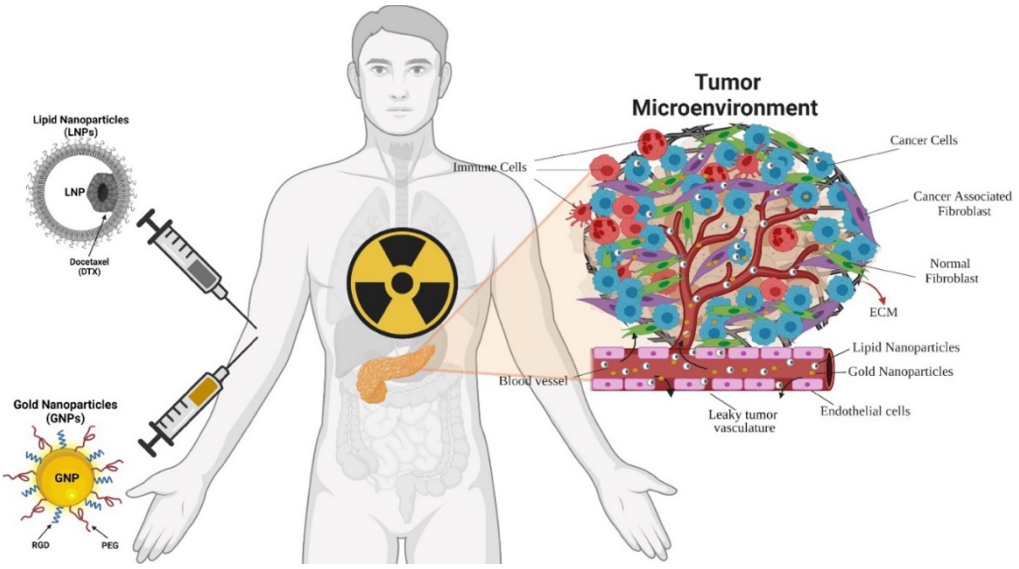

Figure 1. Schematic showing the combined modality of nanotechnology, chemotherapy, and radiotherapy (RT) for treating pancreatic cancer.

The GNPs/RT/$LNP_{DTX\text{-}P}$ combined modality is expected to yield an enhanced therapeutic effect, allowing us to significantly reduce both the RT and chemotherapy doses to spare normal tissues. Subsequently, we evaluated the efficacy of combining clinically relevant doses of GNPs/RT/$LNP_{DTX\text{-}P}$ (Fig. 1) to address the following questions:

How much does the proposed triple combination (GNPs/RT/LNPDTX-P) increase the efficacy of RT alone?

Did $LNP_{DTX\text{-}P}$ show efficacy improvement over free DTX?

How does the effectiveness of the combined treatment compare to the individual effects of each component?

How would our triple combinations of GNPs/RT/DTX and GNPs/RT/$LNP_{DTX\text{-}P}$ compare to high RT doses?

Experimental

Materials and Methods

Gold Nanoparticle Synthesis, Functionalization & Characterization

The citrate reduction method synthesized GNPs measuring approximately 13 nm in size [26]. To visualize the GNPs, images were captured using transmission electron microscopy with an Ultra-high-Resolution Scanning Electron Microscope SU9000 by Hitachi (Pleasanton, CA, United States) as shown in Fig. S1.A. GNPs were functionalized with polyethylene glycol (PEG) and arginine-glycine-aspartic acid (RGD); one PEG molecule per nm^2 of the nanoparticle surface area and one RGD molecule for every two PEG molecules. The attachment of PEG (2000 Da) molecules to GNPs decreases aggregation and minimizes capture by the immune system [27]. On the other hand, RGD with a molecular weight of 1600 Da was used to bind to the αvβ3 integrin receptor, which is overexpressed in pancreatic cancer cells, thus increasing their targeting specificity towards cancer cells [28]. The Perkin Elmer λ 365 UV-Vis spectrophotometer (Waltham, MA, United States) was used to determine the size of the nanoparticles. The size of the nanoparticles with and without PEG, RGD, and LNPs is summarized in Fig. S1.C and shown in Fig. S1.D-E. LiteSizer 500 particle size analyzer (Anton Paar, Graz, Austria) was used to determine the ζ potential and the particle size distribution of our functionalized and non-functionalized nanoparticles (summarized in Fig. S1.C and shown in Fig. S1.F-I), to show their stability.

Lipid Nanoparticle Synthesis

LNPs were made using the methods described in our previous paper [29]. In brief, the LNPs were created using a rapid mixing method. DSPC, PEG-DSPE, cholesterol, and DTX prodrug were dissolved in ethanol to a final lipid concentration of 10 mM and a final molar ratio of 49:1:40:10, respectively. The mixture was then combined with phosphate-buffered saline (PBS) at a flow ratio of 1:4 (v:v) and a 40 mL/min flow rate. After dialysis and sterile filtration, particle size was determined by dynamic light scattering using a Malvern Zetasizer NanoZS (Malvern Instruments, Worcestershire, United Kingdom). Cholesterol and phospholipid content of the LNPs were measured and used to determine the lipid concentration (Cholesterol E Assay, Phospholipids C Assay, Wako Chemicals, Richmond, VA, United States). DTX prodrug quantity was measured using ultra-performance liquid chromatography. Its entrapment in the LNPs was calculated by comparing prodrug cholesterol ratios in the final formulation to the initial lipid mixture. The High-Resolution Macromolecular Cryo-Electron Microscopy Facility at The University of British Columbia performed cryogenic transmission microscopy of the $LNP_{DTX\text{-}P}$ (Fig. S1.B). More information about DTX prodrug synthesis is available in the supplementary section, along with a diagram Fig. S2. DSPC and PEG-DSPE were obtained from Avanti Polar Lipids (Alabaster, AL, United States). The cholesterol used was purchased from Sigma-Aldrich (St. Louis, MO, United States), and DTX was purchased from eNovation Chemicals (Bridgewater, NJ, United States).

Cell Cultures & Spheroid Formation

The MIA PaCa-2 human pancreatic cancer cell line (ATCC#: CRL-1420™) was acquired from the American Type Culture Collection. Human pancreatic cancer-associated fibroblasts (CAF-98) were obtained from a consenting patient's resected pancreatic tumor tissue through the Gastrointestinal (GI) Biobank at Vancouver General Hospital. Both cell types were cultured in high glucose Dulbecco's Modified Eagle's Medium (DMEM; Gibco, Thermo Fisher Scientific, Waltham, MA, USA) supplemented with 10% fetal bovine serum (FBS; Gibco), 1% penicillin/streptomycin (Gibco), and 4 mM GlutaMax (Gibco). Cell detachment was performed using Trypsin-EDTA (Gibco), while cell fixation was achieved using paraformaldehyde (PFA; Sigma-Aldrich, Oakville, ON, Canada). PBS was used for cell washing. Incubation of cells took place at 37°C with 5% CO_2.

For 2D co-culture experiments, cells were seeded at a 5:1 ratio of CAF-98 to MIA PaCa-2 and incubated for three days before initiating the experiments. Regarding 3D spheroid cell cultures, cells were plated in ultra-low attachment 96-well microplates (Corning, NY, United States). Each well contained 6000 cells for MIA PaCa-2 monocultures and 1800 cells for the co-cultures (5:1 ratio of CAF-98 to MIA PaCa-2), resulting in a spheroid size of approx-

imately 400 µm. Cell medium was supplemented with 3% Geltrex matrix (Gibco) on ice to facilitate spheroid formation. For co-culture spheroids, 300 MIA PaCa2 and 1500 CAF-98 cells were seeded per well, and the cells were centrifuged at 350xg for 5 minutes at 4°C. Afterward, they were incubated at 37°C with 5% CO_2. Experiments were initiated once the spheroids had formed, following a 3-day incubation period.

Drug Cytotoxicity Assay

Cytotoxicity assay was used to determine the IC-50 of DTX and $LNP_{DTX\text{-}P}$ in MIA PaCa-2 2D monolayer monocultures and in MIA PaCa-2 monoculture 3D spheroids. For the 2D monoculture, 3 black-walled clear-bottom 96-well plates (Greiner, Kremsmünster, Austria) were used for each drug. Approximately 10000 cells were seeded in each well, and 100 µL of the medium was added, leaving one column empty for control and covered with a breathable membrane to reduce evaporation (Breathe-Easier Membranes, Sigma-Aldrich; St. Louis, Missouri, United States). 24 h post-seeding, the drugs were serially diluted into each column of wells with doses ranging from 1000 nM to 0.01 nM for DTX and 10000 nM to 0.01 nM for $LNP_{DTX\text{-}P}$. After 24 hours of treatment, the membrane was discarded, and the medium in each well was replaced and then rinsed with PBS. Cell viability was assessed 2 days after drug dosing using media containing 10% *v/v* resazurin dye (PrestoBlue, Thermo Fisher, Waltham, MA, USA) following a 30-minute incubation with the dye. Fluorescence was measured using a Biotek Cytation 1 plate reader (Agilent Technologies, Santa Clara, CA, USA) with filters set at Excitation 530/25 nm and Emission 590/35 nm.

Similarly, for the 3D cell culture, once the 3D spheroid models were formed, the drugs were serially diluted into each column of wells with doses ranging from 1000 nM to 0.01 nM for DTX and 10000 nM to 0.01 nM for $LNP_{DTX\text{-}P}$. 24 h post-treatment, approximately half of the medium in each well was removed so as not to disturb the spheroids, rinsed with PBS 5 times, new fresh medium was added, and plates were incubated. 48 h post-incubation, the medium was removed from each well, leaving only 100 µL of medium. Then 30 µL of CellTiter-Glo 3D (Promega, Madison, WI, United States) was added to each well. Following the 0.5 h-incubation period, fluorescence was measured using a Biotek Cytation 1 plate reader (Agilent Technologies, Santa Clara, CA, United States). CellTiter-Glo 3D is a luminescent cell viability assay, which measures the amount of adenosine triphosphate (ATP) present in metabolically active cells. The level of luminescence is directly proportional to the amount of ATP present, which reflects the number of viable cells [30]. PrestoBlue is a colorimetric cell viability assay that measures viable cells' metabolic activity by detecting the reduction of resazurin dye to resorufin. The level of color change is directly proportional to the number of viable cells [31].

Cellular Uptake of Gold Nanoparticle

GNPs and the drugs were dosed concurrently following spheroid formation, and the samples were incubated for 24 h. GNPs were dosed at 7.5 µg/mL, while drugs were dosed at the IC-50 dose found in the previous section: ~100 nM for DTX and ~1000 nM for $LNP_{DTX\text{-}P}$. After the completion of the treatment, the samples underwent a series of steps. Firstly, they were washed with PBS five times and then incubated at 37°C in trypsin-EDTA (Gibco) for 1 hour to facilitate the breakdown of the spheroids. The cells were manually counted using a hemocytometer. Following cell counting, the samples were diluted in 5 mL of Millipore water and then treated with 250 µL of aqua regia for every 500 µL of the sample. The samples were placed in a mineral oil bath at 90°C for approximately 2 hours. Next, 100 µL of hydrogen peroxide was added to each sample, and they were returned to the oil bath for an additional hour. After this, the samples were diluted with deionized water to attain a 2.5% v/v acid content. Lastly, the gold content in each sample was measured using inductively coupled plasma–mass spectrometry (ICP-MS; Agilent 8800 Triple Quadrupole, Agilent Technologies, Santa Clara, CA, United States) like in our previous work [32].

Gold Nanoparticle Imaging

The 3D samples were imaged using a 20× lens of the Confocal microscopy (Zeiss LSM 980, Carl Zeiss Microscopy GmbH, Jena, Germany). The 3D spheroids were treated with GNPs and drugs as described in the previous section. Subsequently, they were transferred to 35 mm coverslip-bottom dishes (MatTek, Ashland, MA, USA) with minimal media to prevent aspiration

and ensure stability during imaging. The GNPs were labeled with Cy5 fluorescent dye molecules to make the gold visible.

Cell Cycle Analysis

Following the spheroids formation, the drugs were administered at the IC-50 dose. The samples were incubated with the drugs for no more than 24 hours, then either the medium was changed or the samples were processed. Following the treatment, the samples were washed with PBS 5 times and incubated at 37°C in trypsin-EDTA (Gibco) for 1 hour to help break down the spheroids. The samples were then rinsed with PBS and centrifuged twice at 350 xg for 5 min. Each sample was washed in 1% PFA and left at 0°C for 15 minutes to be fixed. They were then rinsed in PBS, centrifuged for 5 minutes, and re-suspended in 70% ethanol. To further fixate the cells, the samples must be incubated in the dark at 4°C for 1 hour. After that, a 100-micron cell strainer was used to filter the samples before being centrifuged at 350 xg for 10 minutes at room temperature. All samples were rinsed in 1 mL of 0.5% bovine serum albumin (BSA) and centrifuged for another 5 minutes. A PBTB (PBS, 0.5% BSA, 0.1% Triton-X 100) solution was then used with RNaseA (100 µg/mL) for 25 minutes at room temperature to wash the samples to help degrade the RNA. Propidium iodide (10 µg/mL) was then added, and the samples were incubated for 1 hour before centrifuging at 350 xg for 5 minutes at room temperature. The samples are then suspended in 1 ml of PBS/BSA and filtered through a 50 µm cell strainer. Finally, the samples are run on a flow cytometer (FACS Calibur, BD Biosciences, Franklin Lakes, NJ, USA).

Cell Proliferation Assay & Spheroid Size

After the radiation treatment, a cell proliferation assay was conducted for 3D spheroids at days 1 and 14 post-treatment using CellTiter-Glo 3D (Promega, Madison, WI, United States) and a Biotek Cytation 1 plate reader, following the procedure detailed in the previous sections. To determine the size of the spheroids after treatment, brightfield images of the spheroids were captured every 3 days using the 4× objective of the Biotek Cytation 1 plate reader (Agilent Technologies, Santa Clara, CA, United States). The average diameter of the spheroids was calculated manually with the assistance of ImageJ. The spheroid's perimeter was manually outlined to compute its area (A). The diameter (d) was derived using the formula $d=2(A/\pi)^{0.5}$. While outlining, cell debris resulting from drug or radiation damage was excluded. For each time point, between 8 spheroids were analyzed to determine the average diameter for each condition.

The Bliss Independence principle was used for the evaluation of the potential synergy between GNPs, drugs, and RT [33].

Immunofluorescence Assay

Cells were cultured in 6-well dishes on glass coverslips. The samples were washed with PBS 24 hours after the radiation treatment and then fixed with 4% paraformaldehyde (PFA) for 5 minutes. Subsequently, the cells were rinsed with PBS and washed with 2% BSA/0.1% Triton-X for a 20-minute incubation. To assess DNA double-strand breaks (DSBs), an optically labeled antibody against the repair protein, 53BP1, was used. The 53BP1 primary antibody was diluted 1:200 in 0.5% BSA/0.1% Triton-X/PBS, while the secondary antibody was diluted 1:500 in 0.5% BSA/0.1% Triton-X/PBS. The samples were first incubated with the primary antibody for 1 hour, followed by rinsing with PBS. Then, the samples were washed with 0.5% BSA/0.175% Tween-20/PBS for 5 minutes and incubated with the secondary antibody for 30 minutes in the dark. After the incubation, the samples were washed with PBS and mounted onto glass coverslips using ProLong™ Glass Antifade Mountant and NucBlue™ Fixed Cell ReadyProbes™ Reagent (DAPI) from Invitrogen, Waltham, MA, United States. Imaging of the 53BP1 foci was performed through confocal microscopy (Zeiss LSM 980) using a 60× oil immersion lens. At least 50 nuclei were assessed, and the number of 53BP1 foci indicating DSB foci per cell was measured.

Results

Spheroids & Drug Cytotoxicity

To estimate the efficacy of our $LNP_{DTX\text{-}P}$ (which contains 10 mol% DTX prodrug by weight), CellTiter-Glo 3D (for 3D spheroids) and PrestoBlue (for 2D cultures) assays were used to measure cell viability and cytotoxicity. The IC-50 values were measured to determine

the potency of LNP_{DTX-P} and compare its inhibitory activity to DTX. These values were then used to determine the optimal concentrations of the drugs for our subsequent experiments. Our IC-50 values are shown in Fig.2A-B. The values were only determined for MIA PaCa-2 and not for CAF-98 because the fibroblasts play a supportive role in tumor cell proliferation and growth. For the 2D monolayer, the value of IC-50 of the effective prodrug DTX in LNP_{DTX-P} was ~ 22 nM vs ~ 37 nM for the free DTX. For the 3D spheroids, the IC-50 value of the effective DTX prodrug in the LNP_{DTX-P} was ~ 99 nM vs ~100 nM for the free DTX. The literature confirms huge variations in the value of IC-50 in similar LNP-encapsulated drugs and DTX in pancreatic cancer cells ranging from 1-20 nM [34–36]. These values can vary depending on several factors, such as the experimental conditions, the specific LNP_{DTX} formulation, the assays, and the pancreatic cancer cell line used. However, the increase in IC-50 values shown in the IC-50 value in 3D models for both LNP_{DTX-P} and DTX is consistent with previous experiment reports showing a several-fold increase in IC-50 values from 2D to 3D models [37].

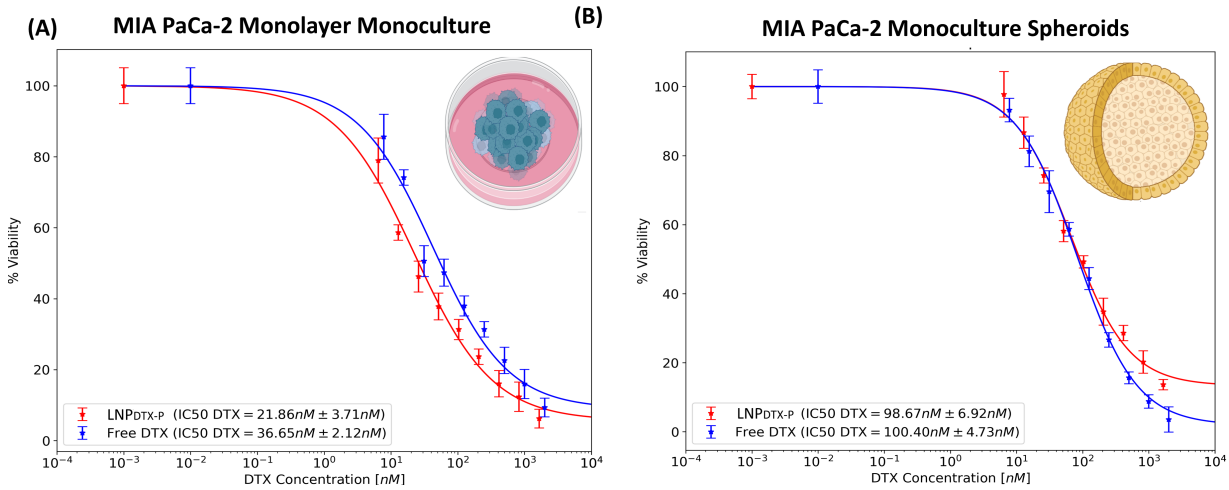

Figure 2. Characterizing drug cytotoxicity. (A–B) Docetaxel (DTX) & LNP_{DTX-P} cytotoxicity proliferation assay for MIA PaCa-2 monolayer monoculture (A) and MIA PaCa-2 monoculture spheroids (B).

LNP_{DTX-P} Effect on Gold Nanoparticles Uptake

The samples were dosed with GNPs (~13 nm in diameter) functionalized with PEG and RGD at a low concentration of 7.5 µg/mL to not induce any potential toxicity from the gold to normal tissues [38]. After an incubation period of 24 h with GNPs and either DTX or LNP_{DTX-P} at the IC-50 concentrations, the medium was changed to mimic the loss of GNPs and drug supply in the body following a single injection. The functionalized GNPs enter cells via receptor-mediated endocytosis, as described in our previous work [39]. The samples were then processed, and the amount of gold in each cell was calculated as described previously. The amount of gold in co-culture cells over time is shown in Fig. 3A. The results show higher levels of gold accumulation in cells co-treated with either DTX or LNPDTX-P compared to cells treated with GNP only. For the co-culture (Fig. 3A), the DTX-treated samples had a 174% (for the LNP_{DTX-P}) and 219% (for the DTX) increase in the amount of gold on the first day of the experiment and retained 65% (for the LNP_{DTX-P}) and 68% (for the DTX) of gold compared to 31% for the non-DTX-treated samples. These results are consistent with the mechanism of action of DTX and other taxane drugs. DTX inhibits microtubule function by promoting tubulin polymerization and inhibiting depolymerization [40]. Microtubules serve many important functions in cells, including acting as "highways" for intracellular transport and playing a critical role in cell division [41]. By disrupting microtubule dynamics, DTX disturbs intracellular transport, decreasing GNP exocytosis and ultimately promoting GNP retention within cells. Furthermore, cell division is inhibited, thus, decreasing GNP distribution into daughter cells. This explains the increase of gold in DTX-treated cells (2-fold increase in amount and over 2-fold increase in retention). These results are supported qualitatively by confocal images of co-culture spheroids (Fig. 3B) over

72 h. It is important to note that our GNPs penetrated into the spheroid's core when combined with DTX and LNP_{DTX-P}. This is most likely because the effects of DTX and LNP_{DTX-P} on the extracellular matrix (ECM) reduce the organization of the ECM, thus aiding in GNP penetration into the core. Moreover, the effects of DTX and LNP_{DTX-P} go beyond increasing the number of GNPs in the spheroid models.

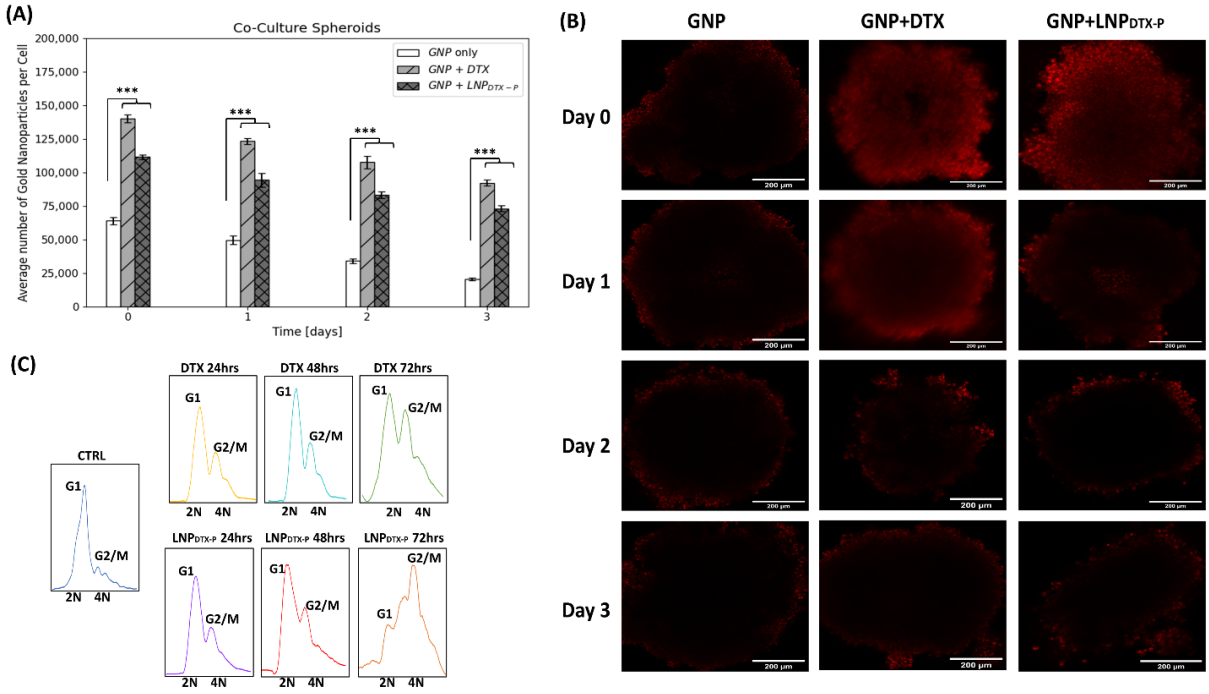

*Figure 3. Gold nanoparticle (GNP) uptake and retention in pancreatic cancer spheroids. (A) Quantification of uptake of 7.5 µg/ml of GNPs into CAF-98 to MIA PaCa-2 (5:1) co-culture spheroids dosed with only GNPs, GNPs + DTX, and GNPs + LNP_{DTX-P}, as measured using ICP-MS. *** indicates $p < 0.001$. (B) Confocal Images of GNPs', in red, uptake, and retention over 3 days in CAF98 to MIA PaCa-2 (5:1) co-culture spheroids dosed with only GNPs (first column), GNPs + DTX (second column), and GNPs + LNP_{DTX-P} (third column). Scale bar: 200 µm. (C) Cell cycle data of co-culture spheroids cells using DTX and LNP_{DTX-P} over 3 days.*

The taxane drug DTX primarily targets cells in the G2/M phase of the cell cycle. It stabilizes microtubules and prevents them from depolymerizing, preventing cells from properly dividing during mitosis [42]. This induces cell cycle arrest, trapping cells in the G2/M phase, which is the most radiosensitive phase of the cell cycle [43]. This synchronized population of G2/M phase cells is the most notable 72 hours post-drug dosing, as seen in Fig. 3C.

The Radiosensitization of Gold Nanoparticles and LNP_{DTX-P}

After an incubation period of 24 hours with the IC-50 concentration of either DTX or LNP_{DTX-P}, the medium was replaced with fresh media, and a single 2 Gy dose was delivered to the samples. Fig. 4A–B displays the relative change in the diameter of co-culture spheroids over 14 days following treatment with and without radiation. When no radiation was used, co-culture spheroids (Fig. 4A) behaved as expected. GNPs for non-irradiated spheroids presented no effects on spheroid size, while DTX and LNP_{DTX-P} caused ~ 12% shrinkage in spheroid size with no significant difference between the two drugs.

On the other hand, the use of GNPs with radiation resulted in ~ 7% spheroid size shrinkage. GNPs/RT/LNP_{DTX-P} resulted in 28% shrinkage in spheroid size. In contrast, GNPs/RT/DTX resulted in 37% shrinkage in spheroid size. These results are visualized using brightfield images of the spheroids 14 days post-treatment (Fig. 4C).

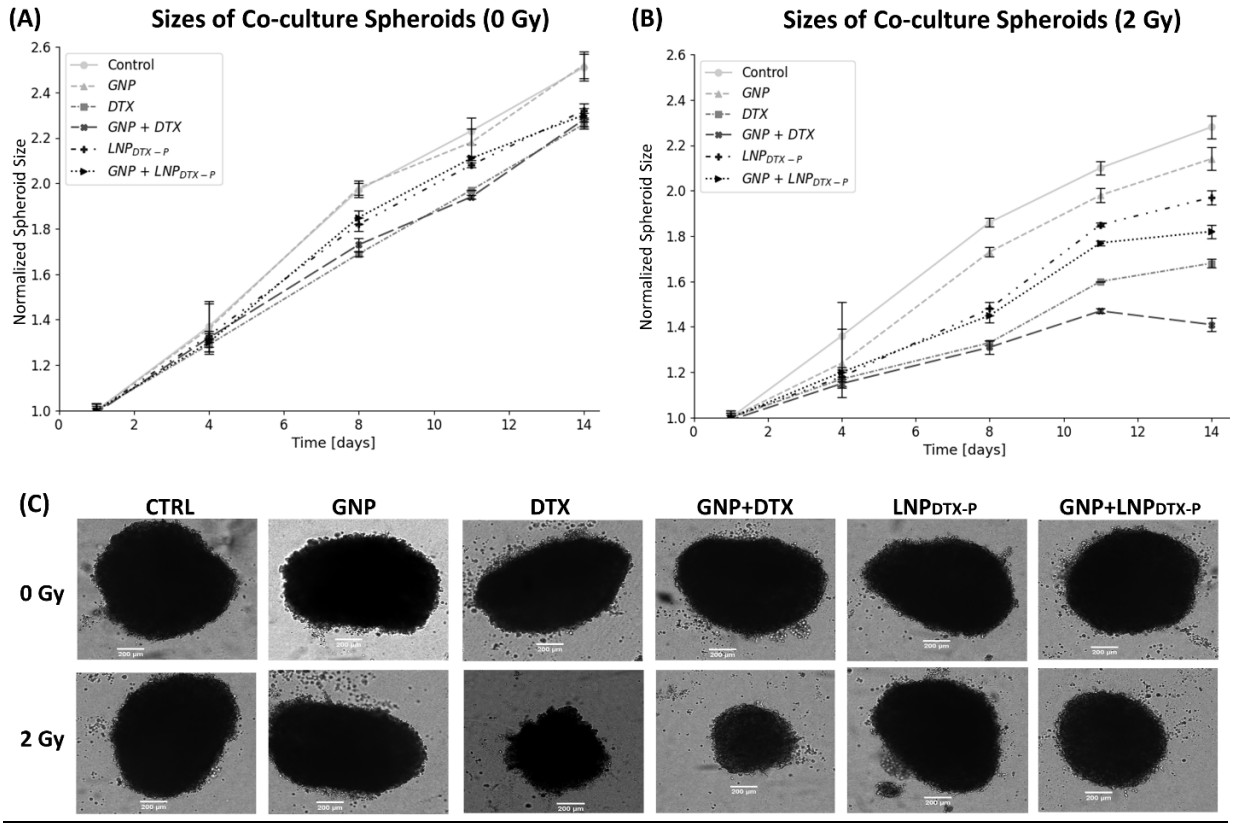

Figure 4. Co-culture spheroids size post-treatment. (A–B) Normalized spheroids sizes over 14 days post-treatment: (A) 0 Gy, (B) 2 Gy. (C) Brightfield images of co-culture spheroids taken 14 days post-treatment. Scale bar: 200 µm.

To corroborate our prior findings, we performed 3D viability assays, as depicted in Fig. S3. The outcomes of these assays align with the results obtained from spheroid size measurements illustrated in Fig. 4A–C. The results show the effectiveness of both DTX and $LNP_{DTX\text{-}P}$ with and without radiation. Without radiation, DTX resulted in a 42% decrease in cell proliferation. However, with radiation and GNPs, DTX showed even further anti-proliferation effects, causing almost a 60% decrease in cell proliferation (Fig. S3). Similarly, $LNP_{DTX\text{-}P}$ resulted in a 34% decrease in cell proliferation with no radiation, while with radiation and GNPs, $LNP_{DTX\text{-}P}$ caused a 46% decrease in cell proliferation (Fig. S3). The two triple combinations of GNPs/RT/DTX and GNPs/RT/$LNP_{DTX\text{-}P}$ showed synergetic effects on the size of the spheroids, while the effect of RT/DTX and RT/$LNP_{DTX\text{-}P}$ was additive (Table 1). It is also worth noting that GNPs by themselves did not cause a toxic effect. This is why the "expected spheroid size" (Table 1) did not change with the addition of GNPs. However, in the presence of radiation, GNPs did cause synergetic effects, albeit less effective than the two triple combinations. These findings indicate the effectiveness of both triple combinations, GNPs/RT/DTX and GNPs/RT/$LNP_{DTX\text{-}P}$, in fighting the increased resistance in a co-culture system. The anticipated outcomes can be attributed to the radiosensitization effects of GNPs. When exposed to ionizing radiation, GNPs can interact with incoming photons and produce secondary electrons through a process known as the photoelectric effect [44]. These secondary electrons have a relatively short range and high energy, which makes them highly damaging to nearby cancer cells and CAFs [44]. The secondary electrons can cause additional ionizations, creating reactive oxygen species (ROS) within the cells. ROS, such as superoxide radicals and hydroxyl radicals, are highly reactive molecules that can induce oxidative stress and damage key cellular components, including proteins, lipids, and DNA.

Table 1. Comparison of the experimentally observed effects of treatments on spheroid size against the anticipated values derived from the Bliss Independence model

	Expected Spheroid Size	Experimental Spheroid Size	Combined Effect
GNPs/RT/DTX	53.52% ± 2.34%	45.59% ± 4.08%	Synergestic***
GNPs/RT/LNP_{DTX-P}	63.39% ± 2.78%	55.21% ± 2.01%	Synergestic***
RT/DTX	53.52% ± 2.34%	52.86% ± 1.95%	Additive**
RT/LNP_{DTX-P}	63.39% ± 2.78%	61.06% ± 2.85%	Additive*
GNPs/RT	93.86% ± 3.56%	84.11% ± 2.71%	Synergestic*

* indicates $p < 0.05$, ** indicates $p < 0.01$, *** indicates $p < 0.001$

This includes interference with DNA repair mechanisms and cell cycle progression, decreasing cell survival and increasing apoptosis [45]. When comparing the performance of DTX to LNP_{DTX-P}, samples treated with DTX had a 26% increase in gold uptake. Both drugs have similar retention effects on cells, retaining roughly 65-70% of the initial gold amount. The effect of both DTX and LNP_{DTX-P} on cell synchronization was nearly identical, but DTX showed better spheroid size control supported by lower cell proliferation. The mechanism of action of DTX was explained in a previous section, and it perfectly supports our results of having an improved therapeutic outcome with the triple combinations of both GNPs/RT/DTX and GNPs/RT/LNP_{DTX-P} in the spheroids.

Although DTX is an effective drug on its own, it can cause severe toxic side effects to normal tissues [35]. To mitigate these side effects, we have developed LNPs that encapsulate DTX prodrugs to deliver them to the target cells more safely and effectively. LNP_{DTX-P} treatment can have certain advantages in lower toxicity and longer circulation time [17–18]. This is because the LNPs can selectively deliver the drug to the tumor, reducing the risk of systemic side effects in other body parts [22–24]. Furthermore, due to a longer circulation time and the EPR effect, more LNP and drug accumulation are expected at the tumor. This may also reduce the level or frequency of dosing required to achieve the therapeutic outcome, improving patient compliance.Additionally, prodrugs of DTX have been shown to improve the bioavailability and solubility of DTX, which can increase its efficacy by improving its cellular uptake, enhancing its stability, and promoting its selective accumulation in tumor cells [46]. DTX prodrug can also reduce systemic toxicity by minimizing exposure to healthy tissues. It is very challenging to observe these effects *in vitro*. It would require further *in vivo* studies because the encapsulation of the drug in NPs without selective targeting results in reduced cellular penetration *in vitro*, while the free drug diffuses more readily into the cells. Therefore, only an in vivo study would allow for an appropriate comparison of these options. We think this explains why LNP_{DTX-P}, with and without GNPs and RT, has a reduced ability to control spheroid size compared to DTX.

DNA Double-strand Breaks (DSBs) in Co-culture

To investigate the impact of radiation on our samples, we conducted an immunofluorescence assay specifically targeting DNA damage. We quantified 53BP1 foci 24 hours after treatment. We visually estimated the average number of DNA DSB foci per cell for different conditions using confocal images highlighting 53BP1 foci in green and the nuclei in blue (Fig. 5A–B). With radiation, there was a minor increase in DNA DSB per cell in co-culture for DTX and LNP_{DTX-P} without GNPs. However, when GNPs were used with the drugs and radiation, we saw a significant increase in DNA DSB (Fig. 5). GNPs with radiation resulted in ~ 20% increase in DNA DSB per cell, GNPs with radiation and DTX resulted in ~42% increase in DNA DSB per cell; GNPs with radiation and LNP_{DTX-P} resulted in ~ 39% increase in DNA DSB per cell. In the absence of radiation, we observed no significant differences between the conditions compared to the control group (Fig. S4). The observed results align with the proposed mechanism of action of GNPs described in previous sections. Coupled with DTX, radiosensitizing increases through cell cycle synchronization in the G2/M phase and increases in GNP accumulation in cells, resulting in higher sensitivity to RT, causing more DNA DSB damage.

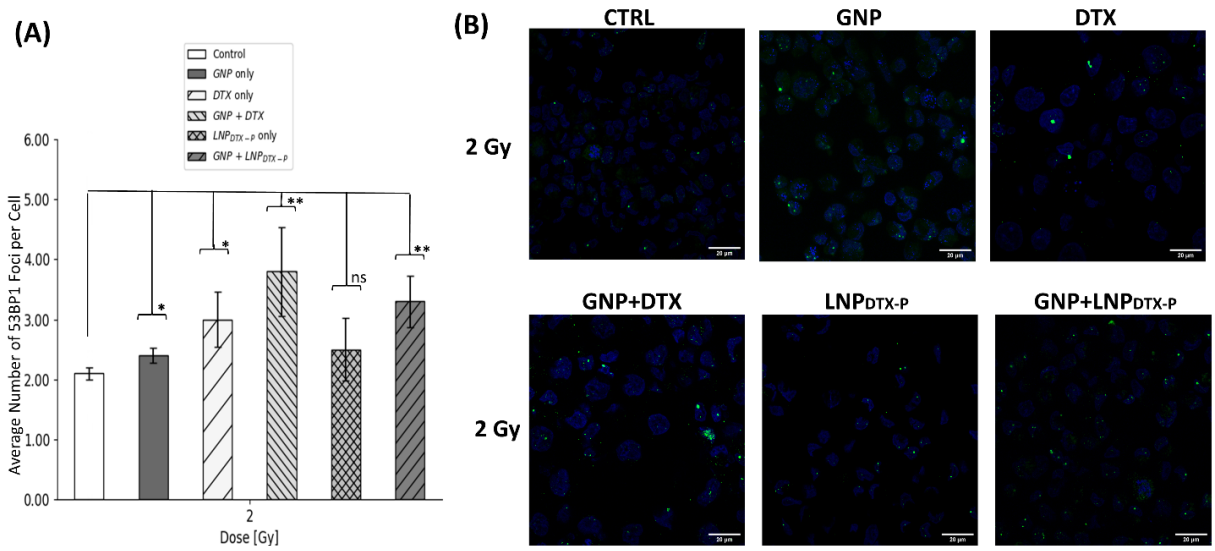

*Figure 5. 2D co-culture repair protein mapping. (A) The average number of 53BP1 per cell in 2D co-culture with radiation following treatments with different agents. ns indicates non-significance, * indicates $p < 0.05$, ** indicates $p < 0.01$. (B) Confocal microscopy images of repair protein 53BP1 in the nucleus of irradiated MIA PaCa-2 and CAF-98 co-cultures. The cell nuclei are stained blue, while the green dots indicate 53BP1 foci—scale bar: 20 µm.*

Gold Nanoparticles/Radiotherapy/LNP_{DTX-P} Combined Treatment in Comparison to Higher Radiotherapy Doses

We compared GNPs/2Gy/LNPDTX-P to 5 Gy and 10 Gy RT to assess the improvement of our triple combined modality compared to RT alone. The aim here is to highlight the effectiveness of the two triple combinations GNPs/RT/DTX and GNPs/RT/LNP_{DTX-P} relative to these elevated radiation doses and to assess if our radiosensitizers (DTX/LNP_{DTX-P} and GNPs) could serve as adequate substitutes for high-dose radiation. The results are shown in Fig. 6.

Samples treated with GNPs/2Gy/DTX were 19% smaller than ones treated with 5 Gy but 8% larger than the ones treated with 10 Gy. In contrast, samples treated with GNPs/2Gy/LNP_{DTX-P} were 6% and 37% larger than ones treated with 5 Gy and 10 Gy, respectively (Fig. 6A). Qualitative brightfield images of the spheroids 14 days post-treatment are shown in Fig. 6B. Immunofluorescence assay shows a significant increase in DNA DSB for both 5 Gy and 10 Gy relative to that of GNPs/2Gy/LNP_{DTX-P} and GNPs/2Gy/DTX (Fig. 6C). Qualitative data showing the results in Fig. 6D. For cell proliferation (Fig. S5), the survival fraction of the samples irradiated with 10 Gy was significantly lower than the rest. However, there was no significant difference between the cell viability of the samples irradiated with 5 Gy and those treated with GNPs/2Gy/DTX. Both had ~20% lower proliferation than the samples treated with GNPs/2Gy/LNP_{DTX-P}. Regarding spheroid size and cell proliferation, it is important to note that adding DTX to RT increases the number of senescent cells [47]. Although these cells are severely damaged, they are not entirely nonfunctional. They may still contribute to the signal through their metabolic activity, add to the size of the spheroid, and not indicate as much DNA DSB damage. Despite that, these results are very promising as they showcase the comparability of both triple combinations of GNPs/RT/DTX and GNPs/RT/LNP_{DTX-P} with high doses of RT. Considering the extra risk of radiation-induced damage to healthy cells surrounding the tumor with higher radiation doses, the combined modality of our two radiosensitizers, GNPs & LNP_{DTX-P} with RT, might represent a more favorable option that would achieve similar results with lower toxicity.

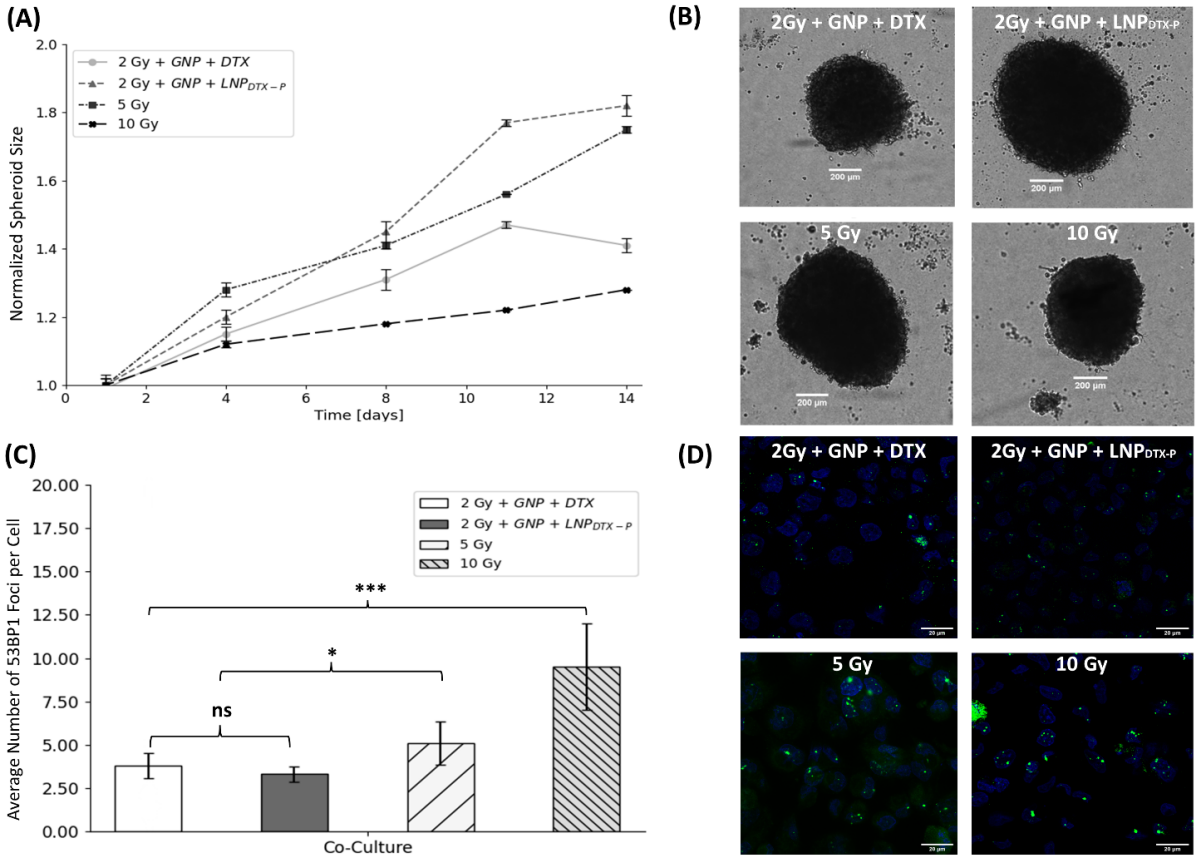

*Figure 6. Irradiated co-culture spheroids. (A) Normalized irradiated co-culture spheroids size over 14 days post-treatment. (B) Brightfield images of irradiated co-culture spheroids taken 14 days post-treatment. Scale bar: 200 µm. (C) Irradiated 2D co-culture indicates the average number of 53BP1 foci per cell. ns indicates non-significance, * indicates $p < 0.05$, *** indicates $p < 0.001$. (D) Confocal microscopy images of repair protein 53BP1 in the nucleus of co-culture of MIA PaCa-2 and CAF-98. Scale bar: 20 µm. The cell nuclei are stained blue, while the green dots indicate 53BP1 foci.*

Conclusions

An *in vitro* 3D co-culture spheroid model consisting of MIA PaCa-2 cancer cells and pancreatic patient-derived cancer-associated fibroblasts (CAF-98) was used to evaluate the efficacy of combining clinically relevant doses of GNPs/RT/LNP$_{DTX-P}$. The findings of this study demonstrate the therapeutic benefits of utilizing GNPs and LNP$_{DTX-P}$ in combination with RT, highlighting their superiority compared to RT alone. GNPs functionalized with PEG and RGD demonstrate promising capabilities as radiosensitizers by improving the efficacy of RT through the production of damaging ROS in tumor cells. LNPs, on the other hand, can improve the effectiveness of the chemotherapy drug docetaxel (DTX) by encapsulating DTX prodrug to create LNP$_{DTX-P}$ and delivering it directly to cancer cells, reducing side effects and improving outcomes. DTX increased the uptake and retention of gold radiosensitizers in the cells and aided cell synchronization at the most radiosensitive phase. ROS production, DNA damage, and cell cycle arrest induced by GNPs/LNPDTX-P/RT produce enhanced radiosensitivity in cancer cells and CAFs. Hence, this triple combination significantly reduced cell survival and spheroid size. Additionally, we showed that radiosensitizers may reduce the overall radiation dose needed to achieve the same therapeutic effect, thereby decreasing the risk of untoward radiation damage and side effects. This synergetic interaction between GNPs, LNP$_{DTX-P,}$ and RT offers the potential for improved therapeutic outcomes in cancer treatment, as it targets both tumor cells and the tumor microenvironment.

Availability of data and materials

Datasets generated and analyzed during the current study are available from the corresponding author upon reasonable request.

Competing interests

Yuen Yi C. Tam is a co-founder and CEO of Integrated Nanotherapeutics, while Sam Chen is a co-founder and director of formulation development at Integrated Nanotherapeutics. Other authors declare no competing interests. For signed statements, please write to the journal office editor@precisionnanomedicine.com.

Funding

This work was supported by the Kuwait Foundation for the Advancement of Sciences under project code CB21-63SP-01, NanoMedicines Innovation Network Strategic Initiative fund (NMIN-SI), a member of the Networks of Centres of Excellence Canada program, the John R. Evans Leaders Fund (JELF) from the Canada Foundation for Innovation, British Columbia Knowledge Development Fund, the Discovery grant from the Natural Sciences and Engineering Research Council of Canada, the National Institutes of Health of United States of America under grants code R01CA257241, R01DE028105, R21CA252156 and R01CA274415, and a collaborative health grant from the University of Victoria.

Authors' contributions

Idea Conceptualization & Methodology: A. A. & D. B. C. Funding Acquisition: A. A., S. K., & D. B. C. Resources: S. C., C. T., & D. B. C. Data Acquisition & Formal Analysis: A. A., R. C., N. J., & J. M. Supervision & Project Administration: W. B., S. K., & D. B. C. Writing Original Draft: A. A. Review & Editing: All authors.

Acknowledgments

The authors would like to acknowledge the support from the University of British Columbia, BC Cancer (Vancouver & Victoria), Pancreas Centre BC, and Integrated Nanotherapeutics Inc.

Quote this article as Alhussan A, Calisin R, Jackson N, Morgan J, Chen S, Tam YYC, Beckham W, Krishnan S, Chithrani DB, A Synergetic Approach Utilizing Nanotechnology, Chemotherapy, and Radiotherapy for Pancreatic Cancer Treatment, Precis. Nanomed. 2023, 6(4):1157-1172, https://doi.org/10.33218/001c.90447

References

1. Siegel, R. L., Miller, K. D., Fuchs, H. E., & Jemal, A. (2022). Cancer statistics, 2022. CA: A Cancer Journal for Clinicians, 72(1), 7–33. https://doi.org/10.3322/caac.21708
2. Bray, F., Ferlay, J., Soerjomataram, I., Siegel, R. L., Torre, L. A., & Jemal, A. (2018). Global cancer statistics 2018: GLOBOCAN estimates of incidence and mortality worldwide for 36 cancers in 185 countries. CA: A Cancer Journal for Clinicians, 68(6), 394-424. doi:10.3322/caac.21492
3. Tempero, M. A., Malafa, M. P., Chiorean, E. G., Czito, B., Scaife, C., Narang, A. K., ... & Zalupski, M. M. (2019). Pancreatic adenocarcinoma, version 1.2019. Journal of the National Comprehensive Cancer Network, 17(3), 202-210. doi:10.6004/jnccn.2019.0017
4. Conroy, T., Hammel, P., Hebbar, M., Abdelghani, M. B., Wei, A. C., Raoul, J. L., ... & Louvet, C. (2018). FOLFIRINOX or gemcitabine as adjuvant therapy for pancreatic cancer. New England Journal of Medicine, 379(25), 2395-2406. doi:10.1056/NEJMoa1809775
5. Ferrone, C. R., Marchegiani, G., Hong, T. S., Ryan, D. P., Deshpande, V., McDonnell, E. I., ... & Warshaw, A. L. (2015). Radiological and surgical implications of neoadjuvant treatment with FOLFIRINOX for locally advanced and borderline resectable pancreatic cancer. Annals of Surgery, 261(1), 12-17. doi:10.1097/SLA.0000000000000798
6. Raucher, D. (2019). Tumor targeting peptides: Novel therapeutic strategies in glioblastoma. Current Opinion in Pharmacology, 47, 14–19. https://doi.org/10.1016/j.coph.2019.01.006
7. Chauhan, V. P., Stylianopoulos, T., Boucher, Y., & Jain, R. K. (2011). Delivery of molecular and nanoscale medicine to tumors: Transport barriers and strategies. Annual Review of Chemical and Biomolecular Engineering, 2, 281-298. doi:10.1146/annurev-chembioeng-061010-114300

8. Burgess, L., Roy, S., Morgan, S., & Malone, S. (2021). A Review on the Current Treatment Paradigm in High-Risk Prostate Cancer. Cancers, 13(17), 4257. https://doi.org/10.3390/cancers13174257
9. Baskar, R., Lee, K. A., Yeo, R., & Yeoh, K.-W. (2012). Cancer and Radiation Therapy: Current Advances and Future Directions. International Journal of Medical Sciences, 9(3), 193–199. https://doi.org/10.7150/ijms.3635
10. Zhou, C., Hao, G., Thomas, P., Liu, J., Yu, M., Sun, S., ... & Zheng, J. (2012). Near-infrared emitting radioactive gold nanoparticles with molecular pharmacokinetics. Angewandte Chemie International Edition, 51(34), 8340-8344. doi:10.1002/anie.201203053
11. Kashyap, B. K., Singh, V. V., Solanki, M. K., Kumar, A., Ruokolainen, J., & Kesari, K. K. (2023). Smart Nanomaterials in Cancer Theranostics: Challenges and Opportunities. ACS Omega, 8(16), 14290–14320. https://doi.org/10.1021/acsomega.2c07840
12. Yao, Y., Zhou, Y., Liu, L., Xu, Y., Chen, Q., Wang, Y., Wu, S., Deng, Y., Zhang, J., & Shao, A. (2020). Nanoparticle-Based Drug Delivery in Cancer Therapy and Its Role in Overcoming Drug Resistance. Frontiers in Molecular Biosciences, 7, 193. https://doi.org/10.3389/fmolb.2020.00193
13. Hainfeld, J. F., Slatkin, D. N., & Smilowitz, H. M. (2014). The use of gold nanoparticles to enhance radiotherapy in mice. Physics in Medicine & Biology, 58(14), 21-36. doi:10.1088/0031-9155/58/14/21
14. Cho, S. H. (2005). Estimation of tumor dose enhancement due to gold nanoparticles during typical radiation treatments: A preliminary Monte Carlo study. Physics in Medicine and Biology, 50(15), N163-173. https://doi.org/10.1088/0031-9155/50/15/N01
15. Li, Z., Huang, P., Zhang, X., Lin, J., Yang, S., Liu, B., Gao, F., Xi, P., Ren, Q., & Cui, D. (2010). RGD-Conjugated Dendrimer-Modified Gold Nanorods for in Vivo Tumor Targeting and Photothermal Therapy. Molecular Pharmaceutics, 7(1), 94–104. https://doi.org/10.1021/mp9001415
16. Cruz, E., & Kayser, V. (2019). Synthesis and Enhanced Cellular Uptake In Vitro of Anti-HER2 Multifunctional Gold Nanoparticles. Cancers, 11(6), 870. https://doi.org/10.3390/cancers11060870
17. Mehta, M., Bui, T. A., Yang, X., Aksoy, Y., Goldys, E. M., & Deng, W. (2023). Lipid-Based Nanoparticles for Drug/Gene Delivery: An Overview of the Production Techniques and Difficulties Encountered in Their Industrial Development. ACS Materials Au. https://doi.org/10.1021/acsmaterialsau.3c00032
18. García-Pinel, B., Porras-Alcalá, C., Ortega-Rodríguez, A., Sarabia, F., Prados, J., Melguizo, C., & López-Romero, J. M. (2019). Lipid-Based Nanoparticles: Application and Recent Advances in Cancer Treatment. Nanomaterials, 9(4), 638. https://doi.org/10.3390/nano9040638
19. Miller, K. D., Nogueira, L., Mariotto, A. B., Rowland, J. H., Yabroff, K. R., Alfano, C. M., Jemal, A., Kramer, J. L., & Siegel, R. L. (2019). Cancer treatment and survivorship statistics, 2019. CA: A Cancer Journal for Clinicians, 69(5), 363-385. doi:10.3322/caac.21565
20. Parodi, A., Buzaeva, P., Nigovora, D., Baldin, A., Kostyushev, D., Chulanov, V., Savvateeva, L. V., & Zamyatnin, A. A. (2021). Nanomedicine for increasing the oral bioavailability of cancer treatments. Journal of Nanobiotechnology, 19, 354. https://doi.org/10.1186/s12951-021-01100-2
21. Zhigaltsev, I. V., Winters, G., Srinivasulu, M., Crawford, J., Wong, M., Amankwa, L., Waterhouse, D., Masin, D., Webb, M., Harasym, N., Heller, L., Bally, M. B., Ciufolini, M. A., Cullis, P. R., & Maurer, N. (2010). Development of a weak-base docetaxel derivative that can be loaded into lipid nanoparticles. Journal of Controlled Release: Official Journal of the Controlled Release Society, 144(3), 332–340. https://doi.org/10.1016/j.jconrel.2010.02.029
22. Chaturvedi, S., Verma, A., & Saharan, V. A. (2020). Lipid Drug Carriers for Cancer Therapeutics: An Insight into Lymphatic Targeting, P-gp, CYP3A4 Modulation and Bioavailability Enhancement. Advanced Pharmaceutical Bulletin, 10(4), 524–541. https://doi.org/10.34172/apb.2020.064
23. Lu, H., Zhang, S., Wang, J., & Chen, Q. (2021). A Review on Polymer and Lipid-Based Nanocarriers and Its Application to Nano-Pharmaceutical and Food-Based Systems. Frontiers in Nutrition, 8, 783831. https://doi.org/10.3389/fnut.2021.783831
24. da Rocha, M. C. O., da Silva, P. B., Radicchi, M. A., Andrade, B. Y. G., de Oliveira, J. V., Venus, T., Merker, C., Estrela-Lopis, I., Longo, J. P. F., & Báo, S. N. (2020). Docetaxel-loaded solid lipid nanoparticles prevent tumor growth and lung metastasis of 4T1 murine mammary carcinoma cells. Journal of Nanobiotechnology, 18, 43. https://doi.org/10.1186/s12951-020-00604-7

25. Khan, M. M., & Torchilin, V. P. (2022). Recent Trends in Nanomedicine-Based Strategies to Overcome Multidrug Resistance in Tumors. Cancers, 14(17), 4123. https://doi.org/10.3390/cancers14174123
26. Bastus, N. G., Comenge, J., & Puntes, V. (2011). Kinetically controlled seeded growth synthesis of citrate-stabilized gold nanoparticles of up to 200 nm: Size focusing versus ostwald ripening. Langmuir, 27(17), 11098-11105. doi:10.1021/la201944z
27. Olivier, J.-C., Huertas, R., Lee, H., Calon, F., & Pardridge, W. (2002). Synthesis of PEGylated immune nanoparticles. Pharmaceutical Research, 19, 1137–1143. https://doi.org/10.1023/A:1019842024814
28. Li, Z., Huang, P., Zhang, X., Lin, J., Yang, S., Liu, B., Gao, F., Xi, P., Ren, Q., & Cui, D. (2010). RGD-Conjugated Dendrimer-Modified Gold Nanorods for in Vivo Tumor Targeting and Photothermal Therapy. Molecular Pharmaceutics, 7(1), 94–104. https://doi.org/10.1021/mp9001415
29. Alhussan, A., Jackson, N., Eaton, S., Santos, N. D., Barta, I., Zaifman, J., Chen, S., Tam, Y. Y. C., Krishnan, S., & Chithrani, D. B. (2022). Lipid-Nanoparticle-Mediated Delivery of Docetaxel Prodrug for Exploiting Full Potential of Gold Nanoparticles in the Treatment of Pancreatic Cancer. Cancers, 14(24), 6137. https://doi.org/10.3390/cancers14246137
30. Booij, T. H., Price, L. S., & Danen, E. H. J. (2019). 3D Cell-Based Assays for Drug Screens: Challenges in Imaging, Image Analysis, and High-Content Analysis. Slas Discovery, 24(6), 615–627. https://doi.org/10.1177/2472555219830087
31. Xu, M., McCanna, D. J., & Sivak, J. G. (2015). Use of the viability reagent PrestoBlue in comparison with alamarBlue and MTT to assess the viability of human corneal epithelial cells. Journal of Pharmacological and Toxicological Methods, 71, 1–7. https://doi.org/10.1016/j.vascn.2014.11.003
32. Alhussan, A., Palmerley, N., Smazynski, J., Karasinska, J., Renouf, D. J., Schaeffer, D. F., Beckham, W., Alexander, A. S., & Chithrani, D. B. (2022). Potential of Gold Nanoparticles in Current Radiotherapy Using a Co-Culture Model of Cancer Cells and Cancer Associated Fibroblasts. Cancers, 14(15), Article 15. https://doi.org/10.3390/cancers14153586
33. Amzallag, A., Ramaswamy, S., & Benes, C. H. (2019). Statistical assessment and visualization of synergies for large-scale sparse drug combination datasets. BMC Bioinformatics, 20(1), 83. https://doi.org/10.1186/s12859-019-2642-7
34. Xiang, S., Sarem, M., Shah, S., & Shastri, V. P. (2018). Liposomal Treatment of Cancer Cells Modulates Uptake Pathway of Polymeric Nanoparticles by Altering Membrane Stiffness. Small (Weinheim an Der Bergstrasse, Germany), 14(14), e1704245. https://doi.org/10.1002/smll.201704245
35. Feng, X., Xiong, X., & Ma, S. (2022). Docetaxel-Loaded Novel Nano-Platform for Synergistic Therapy of Non-Small Cell Lung Cancer. Frontiers in Pharmacology, 13, 832725. https://doi.org/10.3389/fphar.2022.83272
36. Yang, L., Gong, L., Wang, P., Zhao, X., Zhao, F., Zhang, Z., Li, Y., & Huang, W. (2022). Recent Advances in Lipid Nanoparticles for Delivery of mRNA. Pharmaceutics, 14(12), 2682. https://doi.org/10.3390/pharmaceutics14122682
37. Bromma, K., Dos Santos, N., Barta, I., Alexander, A., Beckham, W., Krishnan, S., & Chithrani, D. B. (2022). Enhancing nanoparticle accumulation in two-dimensional, three-dimensional, and xenograft mouse cancer cell models in the presence of docetaxel. Scientific Reports, 12(1), Article 1. https://doi.org/10.1038/s41598-022-17752-5
38. Khlebtsov, N., & Dykman, L. (2011). Biodistribution and toxicity of engineered gold nanoparticles: A review of in vitro and in vivo studies. Chemical Society Reviews, 40(3), 1647–1671. https://doi.org/10.1039/c0cs00018c
39. Alhussan, A., Bromma, K., Perez, M. M., Beckham, W., Alexander, A. S., Howard, P. L., & Chithrani, D. B. (2021). Docetaxel-Mediated Uptake and Retention of Gold Nanoparticles in Tumor Cells and in Cancer-Associated Fibroblasts. Cancers, 13(13), 3157. https://doi.org/10.3390/cancers13133157
40. Jain, S., Hirst, D. G., & O'Sullivan, J. M. (2012). Gold nanoparticles as novel agents for cancer therapy. The British Journal of Radiology, 85(1010), 101–113. https://doi.org/10.1259/bjr/59448833

41. Steinberg, G., & Fuchs, U. (2004). The role of microtubules in cellular organization and endocytosis in the plant pathogen Ustilago maydis. Journal of Microscopy, 214(Pt 2), 114–123. https://doi.org/10.1111/j.0022-2720.2004.01319.x
42. Hu, J., Chen, L., Lu, Z., Yao, H., Hu, Y., Feng, L., Pang, Y., Wu, J.-Q., Yu, Z., & Chen, W.-H. (2023). Design, Synthesis and Antitumor Activity of Novel Selenium-Containing Tepotinib Derivatives as Dual Inhibitors of c-Met and TrxR. Molecules (Basel, Switzerland), 28(3), 1304. https://doi.org/10.3390/molecules28031304
43. Krueger, S. A., Wilson, G. D., Piasentin, E., Joiner, M. C., & Marples, B. (2010). THE EFFECTS OF G2-PHASE ENRICHMENT AND CHECKPOINT ABROGATION ON LOW-DOSE HYPER-RADIOSENSITIVITY. International Journal of Radiation Oncology, Biology, Physics, 77(5), 10.1016/j.ijrobp.2010.01.028. https://doi.org/10.1016/j.ijrobp.2010.01.028
44. Guo, M., Sun, Y., & Zhang, X.-D. (2017). Enhanced Radiation Therapy of Gold Nanoparticles in Liver Cancer. Applied Sciences, 7(3), Article 3. https://doi.org/10.3390/app7030232
45. Tan, J., Cho, T. J., Tsai, D.-H., Liu, J., Pettibone, J. M., You, R., Hackley, V. A., & Zachariah, M. R. (2018). Surface Modification of Cisplatin-complexed Gold Nanoparticles and its Influence on Colloidal Stability, Drug Loading and Release. Langmuir : The ACS Journal of Surfaces and Colloids, 34(1), 154–163. https://doi.org/10.1021/acs.langmuir.7b02354
46. Wu, R., Zhang, Z., Wang, B., Chen, G., Zhang, Y., Deng, H., Tang, Z., Mao, J., & Wang, L. (2020). Combination Chemotherapy of Lung Cancer – Co-Delivery of Docetaxel Prodrug and Cisplatin Using Aptamer-Decorated Lipid–Polymer Hybrid Nanoparticles. Drug Design, Development and Therapy, 14, 2249. https://doi.org/10.2147/DDDT.S246574
47. Zhu, S., Oremo, J. A., Li, S., Zhen, M., Tang, Y., & Du, Y. (2014). Synergistic Antitumor Activities of Docetaxel and Octreotide Associated with Apoptotic-Upregulation in Castration-Resistant Prostate Cancer. PLOS ONE, 9(3), e91817. https://doi.org/10.1371/journal.pone.0091817